Elsevier Editorial System(tm) for Journal of Magnetism and Magnetic Materials
Manuscript Draft

Manuscript Number:

Title: The influence of Nd-Co substitution on non-stoichiometric strontium hexaferrite nanoparticles

Article Type: Regular Submission

Keywords: Srtrontium hexaferrite; Nd-Co substitution; magnetic properties; non-stoichiometric hexaferrite

Corresponding Author: Dr. Paula G. Bercoff, PhD

Corresponding Author's Institution: Facultad de Matemática, Astronomía y Física. Universidad Nacional de Córdoba, Argentina

First Author: Paula G. Bercoff, PhD

Order of Authors: Paula G. Bercoff, PhD; Carlos Herme; Silvia E Jacobo

Abstract: Non-stoichiometric Nd-Co substituted hexaferrites of composition Sr(1-x)NdxFe12(1-x)CoxO19 (x= 0 to 0.4) were prepared by the self-propagating combustion method and subsequent heat treatments. Structural characterization of the samples showed that the M-type hexagonal structure can be maintained for substitutions x<0.4 without segregation of secondary phases on samples calcined at 1100ºC. The crystallites sizes range between 50 and 70 nm. Mössbauer spectroscopy results indicate that the iron vacancies are not evenly distributed over the lattice and that Co/Fe substitution mainly takes place in site 4f2. Magnetic measurements reveal that the values of saturation magnetization Ms increased from 72 to 76 emu/g (x=0-0.2) while coercivity Hc increased from 2100 to 4670 Oe (x=0-0.3). Nd-Co substitutions enhance magnetic properties in deficient iron Sr hexaferrites.

Editor of the

Journal of Magnetism and Magnetic Materials

Dear Editor,

I am sending the paper "*The influence of Nd-Co substitution on non-stoichiometric strontium hexaferrite nanoparticles*" for you to consider for publication at the Journal of Magnetism and Magnetic Materials. This is an original, unpublished paper which is not currently being reviewed elsewhere.

Kindest regards,

Dr. Paula G. Bercoff

* Manuscript
Click here to view linked References

The influence of Nd-Co substitution on non-stoichiometric strontium hexaferrite nanoparticles

P. G. Bercoff[1 *], C. Herme[2] and S. E. Jacobo[2]

[1]Facultad de Matemática, Astronomía y Física, Universidad Nacional de Córdoba, Argentina. IFFaMAF, Conicet, Argentina.

[2]LAFMACEL, Facultad de Ingeniería, UBA, Paseo Colón 850, C1063EHA, Buenos Aires, Argentina.

[*] Corresponding author

Abstract

Non-stoichiometric Nd-Co substituted hexaferrites of composition $Sr_{1-x}Nd_xFe_{12(1-x)}Co_xO_{19}$ (x= 0 to 0.4) were prepared by the self-propagating combustion method and subsequent heat treatments. Structural characterization of the samples showed that the M-type hexagonal structure can be maintained for substitutions x<0.4 without segregation of secondary phases on samples calcined at 1100ºC. The crystallites sizes range between 50 and 70 nm. Mössbauer spectroscopy results indicate that the iron vacancies are not evenly distributed over the lattice and that Co/Fe substitution mainly takes place in site 4f2. Magnetic measurements reveal that the values of saturation magnetization M_S increased from 72 to 76 emu/g (x=0-0.2) while coercivity Hc increased from 2100 to 4670 Oe (x=0-0.3). Nd-Co substitutions enhance magnetic properties in deficient iron Sr hexaferrites.

1. Introduction

Hexagonal ferrites have been widely used as permanent magnets since their discovery in the 1950s. In spite of their relatively modest magnetic properties, ferrite magnets still show the best cost-to-ratio performance [1]. So far, tremendous efforts have been made in improving their magnetic capabilities by using different synthesis methods [2-4]. In M-type hexaferrites, the 24 iron atoms of a unit cell occupy five different crystallographic sites: three octahedral sites, crystallographically known as 2a, 12k, and $4f_2$, one tetrahedral site ($4f_1$) and one bipyramidal site (2b). In the magnetically ordered state in $BaFe_{12}O_{19}$ or $SrFe_{12}O_{19}$, the 12k, 2a and 2b sites have their spins aligned parallel to each other and to the crystallographic c-axis, whereas those of $4f_2$ and $4f_1$, point in the opposite direction.

Different routes have been tried to prepare nanosized single-domain particles [5-8]. In most cases the attempt to get single-phase materials failed when the heat-treatment temperature remained below 1200ºC, giving large multi-domain particles not suitable for recording applications.

It has been reported that the saturation magnetization as well as the magnetocrystalline anisotropy constant of magnetoplumbite ferrite fine particles were increased by the substitution of La-Co ions [9, 10]. Different scientific investigations and techniques (Mössbauer spectrometry, X-ray diffraction and magnetic measurements) have allowed to optimize the permanent magnet properties of La-Co substituted hard ferrite magnets with the $Sr_{1-x}La_xFe_{12-y}Co_yO_{19}$ composition. For y=x, the magnetic properties increase up to x=0.2 and then decrease due to the presence of secondary La and Co containing phases and to lateral grain growth during sintering [11]. It has also been observed that La excess induces the decoupling of the particles, thus enhancing the coercivity [12]. However, the solubility of rare earth ions in Sr-hexaferrites is very low and their introduction in the stoichiometry leads to the formation of secondary phases, which must be avoided in order to obtain permanent magnets with optimal properties.

J. F. Wang *et al.* have investigated hydrotermally synthesised Sm-doped Sr hexaferrite particles [13]. They found that, unlike transition metals substitution, Sm substitution does not decrease the hexaferrite particle size. The intrinsic coercivities of Sm-doped Sr hexaferrites are significantly higher than those of Sr hexaferrite. By the same chemical route, Wang *et al.* prepared Nd-substituted Sr hexaferrite [14]. They reported that for Nd-Sr ratios up to 1/8, the saturation magnetization values M_s are almost the same as that of the undoped ferrite, whereas their coercivities are around 11% higher. In both papers secondary phases such as $SrFeO_3$ and $NdFeO_3$ were observed for all the Sr-rare earth ions substitution. Recently, L. Lechevalier *et al.* [15] reported the results on the structural investigation of $Sr_{1-x}R_xFe_{12}O_{19}$ and $Sr_{1-x}R_xFe_{12-x}Co_xO_{19}$ hexaferrite powders (R=rare earth) and discussed the influence of the presence of Co on the rare-earth ions solubility in the M-type phase.

The citrate self-combustion route has been tried for La-Co substituted hexagonal ferrite [16]. However, complete single-phase formation was not observed for annealing temperatures below 1200°C.

In this paper the novel results on the synthesis and characterization of Sr ferrites with Nd-Co substitution are presented. Since different iron compounds have been reported to be the main secondary phases when rare earth ions substitution increases [15], a deficient iron formulation is proposed. The structural and magnetic analysis of $Sr_{1-x}Nd_xFe_{12(1-x)}Co_xO_{19}$ (x= 0 to 0.40) prepared by the self-combustion method is presented.

2. Experimental

Samples of composition $Sr_{1-x}Nd_xFe_{12(1-x)}Co_xO_{19}$ (x= 0.00; 0.10; 0.20; 0.30 and 0.40, labeled N0, N10, N20, N30 and N40, respectively) were prepared by the self-combustion method. The chemical precursors used for these experiments were $Fe(NO_3)_3 \cdot 9H_2O$, $SrCO_3$, Nd_2O_3, $Co(CH_3COO)_2 \cdot 4\ H_2O$. The precursors were weighed according to different Nd^{3+}-Sr^{2+} - Fe-Co mole ratios and completely dissolved in small amounts of a nitric acid solution. Then, the pH was

adjusted to about 7 by adding ammonium hydroxide. When the citric acid ($COH(CH_2COOH)_2COOH$) was added, the result was a sol of metal hydroxides and ammonium nitrate. The ratio citri:nitric acid was fixed in 2:1 for each experiment. Aqueous suspensions were stirred and heated for several hours until the sol turned into a dried gel. Then the dried gel was ignited in a corner and a combustion wave spontaneously propagated through the whole gel converting it into loose magnetic powder. After quick combustion, the powder was heat-treated at 400ºC for one hour to eliminate the residual organic compound. Then, the powders were calcined in air at 800 and 1100ºC for two hours. In order to identify the calcined samples, the temperature of calcination was added at the end of each sample label. The non-stoichiometric compositions and sample labels for the powders heated at 1100ºC are given in Table 1. The oxigen content was calculated assuming the following valences: Sr^{2+}, Nd^{3+}, Co^{2+} and Fe^{3+}.

Table 1

The structural analysis of the powders was done by X-ray diffraction using a Philips diffractometer and CuKα radiation. The patterns were taken between 2θ=20º and 70º with a step of 0.02º. The average size of the crystals (D) was estimated using Scherrer´s formula considering only the (110), (107), (114) and (203) reflections. Cell parameters were calculated using the program TREOR. A vibrating sample magnetometer Lakeshore 7200 was used to measure the magnetic properties at room temperature. The different powders were compacted into disks of 6 mm in diameter and 1 mm thick so as to fit in the sample holder of the VSM magnetometer, keeping a low thickness-to-diameter ratio in order to avoid demagnetizing fields. Hysteresis loops M vs H were measured with a maximum applied field of 15 kOe. Since the loops did not saturate at 15 kOe, the value of saturation magnetization M_S for each sample was calculated by extrapolating to 0 M vs 1/H. Fe Mössbauer spectroscopy was performed at 298K, on the samples calcined at 1100°C. ^{57}Co/Rh was used as a radiation source and a constant acceleration drive. The spectrometer was calibrated by first taking a run of α-Fe foil.

3. Results and Discussion

The X-ray analyses reveal that, in all patterns, the main peaks correspond to the hexagonal M-type phase.

The as-combusted powders calcined at 800ºC for two hours (Figure 1) contain different amounts of the hexaferrite phase (33-0664) −according to the cation defficiency− that range from 30% for N0-800, 50% for N10-800, 90% for N20-800 and 100% for N30-800. Small amounts of hematite α-Fe_2O_3 (33-0664) and maghemite γ-Fe_2O_3 (25-1402) are present in samples with $x<0.2$. Neither the orthoferrite phase $SrFeO_3$ (17-0932) nor neodymium oxide Nd_2O_3 (43-1023) were detected in any of the samples calcined at the mentioned temperature. Sample N40-800 contains

60% of the hexagonal phase and other iron oxides such as $SrFeO_{2.5}$ (17-0932) are present. Crystallite sizes are 40-45 nm, and a slight decrease is observed with substitution.

All the samples calcined at 1100ºC for two hours show the characteristic diffraction patterns of an hexagonal phase with crystallite sizes that decrease from 70 nm to 55 nm (Figure 2) with increasing substitution. Table 1 shows that cell parameters are modified with substitution. Parameters $a=b$ increase with x while parameter c slightly increases up to x=0.10 and then decreases for iron vacancies greater than 9%. These results confirm that Nd and Co ions can easily enter the lattice while keeping the hexagonal structure rather unchanged. Cell parameters for sample N40 (not shown) indicate a monoclinic structure, possibly due to the high substitution and the high iron vacancies (40%) in this sample. For N0-1100 and N10-1100 extra peaks from hematite α-Fe_2O_3 appear. Samples labeled N20-1100 and N30-1100 are single-phase. It is very important to remark that by this preparation method, Nd solubility is a high as 3.5 at % (N30-1100). Probably, the presence of vacancies in the composition promotes rapid diffusion of ions during the thermal treatment, so a single-phase compound can be obtained at low temperatures for x=0.2 and x=0.3. In N40-1100 traces of $SrFeO_{2.5}$ (17-0932) and $SrNdFeO_4$ (25-0903) are observed.

Figure 1

Figure 2

The Mössbauer spectra of the samples calcined at 1100ºC have been analyzed in terms of five Zeeman sextets, except for samples N0-1100 and N10-1100 where another contribution from some hematite was included. The intensity of each sextet is directly proportional to the number of iron atoms in each site, thus giving an estimate of the occupancy percentage in the corrsponding site. Figure 3 shows the Mössbauer spectra of sample N30-1100.

Figure 3

Figure 4

Figure 4 shows Fe^{3+} occupancy values of the five sites of $Sr_{1-x}Nd_xFe_{12(1-x)}Co_xO_{19}$ obtained from Mössbauer data. Theoretical values calculated from stoichiometrical formulae are also shown for comparison. Iron vacancies are not proportionally distributed in all sites. The occupancy of sites 12k, 4f2 and 2b is lower than the theoretical values and vary following the same tendency of the theoretical data up to x=0.3. It is observed that the linewidth of the 12k contribution increases with x, in agreement with an increasing distribution of environments around the 12k. This indicates that Co^{2+}/Fe^{3+} substitution occurs in the vecinity of the 12k site, *i.e.* on 4f1, 4f2 or 2a [17]. The inherent

randomness in site occupancy of different ions and presence of vacancies (due to non-stoichiometry) appear to be responsible for the large increase in linewidth.

The low values of 4f2 can be related to Co^{2+}/Fe^{3+} substitution [18]. Both 4f1 and 2a are slightly over the calculated values. It is noticiable that the site occupancy of 2a remarkably decreases from x=0 to x=0.1, suggesting a substitution also in this site.

For x=0.4 Figure 4 shows a high Fe migration from 12k to 2a and 4f2, so a different Fe environment may be expected, as Fe vacancies are as high as 40%.

These results are in accordance with the isomer shift and quadrupolar behavior shown in Figures 5 and 6, respectively.

Figure 5

From Figure 5, a decrease of the isomer shift of 4f2 is observed for x>0. This decrease is attributed to the presence of Nd^{2+} instead of Sr^{2+} in the vicinity of the 4f2 site related to an increase of the electron density around this site [6]. However, as Fe vacancies increase with x, the electronic density is diluted. The decrease in Isomer effect is not monotonically observed for all x because both effects contrarrest each other.

Figure 6

Figure 6 shows that the quadrupole splitting of 12k and 4f1 do not change with x. A slight increase of the quadrupolar shift of the 4f2 contribution up to x=0.2 is observed, while a decrease of the quadrupolar shift of the 2b contribution is noticed. These variations are attributed to a perturbation of the symmetry around these sites due to Nd^{3+}/Sr^{2+} and Co^{2+}/Fe^{3+} substitution, without discarding iron vacancies. For x>0.3 the iron vacancies need to be considered for further analisis.

Figure 7

Figure 8

Figures 7 and 8 show the obtained saturation magnetization M_S and coercivities Hc, respectively, as a function of Nd-Co concentration for the samples calcined at 800 and 1100ºC. Both figures show that Nd-Co substitution increases M_S and Hc. For the powders calcined at 1100 ºC these magnitudes reach a maximum for x= 0.2 and 0.3 respectively. Thermal treatement at 1100ºC promotes grain growth and improves crystallinity. Therefore, saturation magnetization increases while coercivity slightly decreses when comparing to the powders calcined at 800ºC.

The observed increase in M_S is consistent with Co^{2+}/Fe^{3+} substitution of the antiparallel 4f1 or 4f2 ions, considering that the moment of Co^{2+} is smaller than that of Fe^{3+} [19].

The inset in Figure 8 shows the hysteresis loops for the unsubstituted sample (N0-1100) and for N30-1100. The improvement in magnetic properties as a consequence of Nd-Co substitution is clearly noticed, enhancing both saturation magnetization and coercivity. To our knowledge, these results have not been reported by other authors.

Figure 9

A random distribution of Fe^{3+} and O vacancies in the hexagonal lattice after a short thermal treatment may give rise to different magnetic orderings. In order to investigate this possibility, the susceptibility χ of the samples calcined at 1100 ºC was calculated as the derivative of M with respect to H of the superior branch of the hysteresis loop. In order to obtain a good fit of χ in all the samples it was necessary to consider two contributions to magnetization. Figure 9 shows χ *vs* H and the fitting of the experimental data for the mentioned samples. The maxima dM/dH (denoted $_{\chi}H_c$) are listed in Table 2, together with the relative contribution of each peak. These are very high coercivities for Sr ferrite, which has reported values as high as 3400 Oe with La, Gd and Er substitution [5], 4400 Oe [11, 20] and 5000 Oe [18] with La-Co substitution.

Table 2

Both Figure 9 and Table 2 clearly show that there are two contributions to Hc. In all the samples calcined at 1100ºC the only hard magnetic phase is the hexagonal ferrite (Figure 2) so we assign the two magnetic contributions observed in χ to an inhomogeneous cationic distribution which gives rise to two magnetic phases: a more ordered one with the lower coercivity and another with defects and/or vacancies which originate higher anisotropy regions with higher coercivities. This phenomenon has been reported in a recent work on similar samples [21]. Hc results in an intermediate value given by the relative contribution of each magnetic phase (see Table 2) because of the interaction between the two observed magnetic phases.

Samples N0-1100 and N10-1100 have very similar contributions but as x increases to 0.2 and 0.3, Fe content decreases as 12(1-x) originating vacancies that act as pinning centers of the domain walls (samples N20-1100 and N30-1100). For x=0.4 the magnetic dilution is evidenced in the abrupt drop of Hc.

In a work by other authors [12], where Ba hexaferrite with La-Co substitution is studied, a stoichiometric sample with La-Co substitution is compared to one with La excess (which implies an iron deficiency). They observe a very high coercivity of 6700 Oe for the iron-deficient sample and explain this considering that La excess both raises the anisotropy field and decouples the

particles. They also find that hematite is not formed in samples with La excess. In the present case it could be assumed that the responsibles for the high $_{\chi}H_c$ are Nd-Co substitution and an inhomogeneous cationic distribution in the formation process that originates regions of higher anisotropy.

4. Conclusions

Nd-Co substituted hexaferrites $Sr_{1-x}Nd_xFe_{12(1-x)}Co_xO_{19}$ (x= 0 to 0.4) were successfully prepared by the self-propagating combustion method. The main phase observed for samples N20-800 and N30-800 is the hexagonal one with a coercivity as high as 5030 Oe. Calcination of the powders for 2 hours at 1100°C produces a single phase in samples with x<0.4.

Nd solubility is found to be as high as 3.5 at% (for x=0.3). Cell parameters increase with substitution even when iron defficiency rapidly increases. These results confirm that Nd and Co ions can easily enter the lattice while keeping the hexagonal structure unchanged. For x=0.4 the amount of Fe vacancies is as high as 40%, resulting in a breaking down of the hexaferrite structure and apparition of other phases, indicating that the stucture of such a diluted sample is not stable.

Mössbauer investigations confirm that iron vacancies are not evenly distributed in each crystalline site and that Co/Fe substitution mainly takes place in site 4f2, increasing *M*s .
Both Fe and O vacancies favor ion migration and Nd inclusion in the lattice without sensibly modifying the magnetic structure up to x=0.3. Nd-Co substitution greatly enhances coercivity. Saturation magnetization is also improved.

Acknowledgements

The authors are indebted to Bibiana Arcondo for Mössbauer spectra and J. Carpenco for experimental assistance. This work was financially supported by Universidad de Buenos Aires (UBACyT I-055) and Conicet (PIP 6452).

References

[1] H. Kojima, in:E. P. Wohlfarth (Ed.), *Ferromagnetic Materials*, vol.3, North-Holland, Amsterdam, 1982, pp.305-391.

[2] Y. P. Fu, C. H. Lin, *J. All. Comp.* 386 (2005) 222.

[3] X. Lui, W. Zhong, S. Yang, Z. Yu, B. Gu, Y. Du, *Phys. Stat. Sol. A* 193 (2002) 314.

[4] J. M. Le Breton, L. Lechevallier, J. F.Wang, R. Harris, *J. Mag. Mag. Mat*. 272-276 (2004) 2214-2215.

[5] N. Rezlezcu, C. Doroftei, E. Rezlezcu, P. D. Popa, *J. All. Comp*. (2007), doi: 10.1016/j.jallcom.2007.04.102.

[6] L. Lechevallier, J. M. Le Breton, A. Morel, F.Kools, P. Tenaud, *Physica B* 327 (2003) 135-139.

[7] S. E. Jacobo, C. Domingo-Pascual, R. Rodríguez Clemente and M. A. Blesa. *J. Mat. Sci.*, 32, (1997) 1025-1028.

[8] P. G. Bercoff and H. R. Bertorello, *Mat. Sci. Forum,* Vol. 302-303, pp 435-439. Ed. Trans Tech Publications, Ltd., Switzerland, 1999.

[9] H. Taguchi, Y. Minachi, K. Masuzawa, H. Nishio, *Eighth Proceedings of the International Conference on Ferrites* (2000) 405.

[10] F. Kools, A. Morel, R. Grössinger, J. M. Le Breton, P. Tenaud, *J. Mag. Mag. Mat*. 242-245 (2002) 1270-1276.

[11] P. Tenaud, A. Morel, F. Kools, J. M. Le Breton, L. Lechevallier, *J. All. Comp.* 370 (2004) 331-334.

[12] M. I. Oliva, P. G. Bercoff, H. R. Bertorello, *J. Mag. Mag. Mat*. Vol 320/14 (2008) e100-e103.

[13] J. F. Wang, C. B. Ponton, I. R. Harris, *J. Mag. Mag. Mat*. 234 (2001) 233-240.

[14] J. F. Wang, C. B. Ponton, I. R. Harris, *IEEE Trans. Magn*., vol 38, Nº5 (2002).

[15] L. Lechevallier, J. M. Le Breton, A. Morel, P. Tenaud, *J. Mag. Mag. Mat*. 316 (2007) e109-e111.

[16] Q. Fang, H. Bao, D. Fang, J. Wang, X. Li, *J. Mag. Mag. Mat*. 278 (2004) 122-126.

[17] J. M. Le Breton, J.Teillet, G.Wiesinger, A.Morel, F.Kools and P.Tenaud, *IEEE Trans. Mag*. 38, 5 (2002) 2952-2954.

[18] X. Liu, P. Hernández-Gómez, K. Huang, S. Zhou, Y. Wang, X. Cai, H. Sun, B. Ma, *J. Mag. Mag. Mat*., doi: 10.1016/j.jmmm.2006.02.096.

[19] M. W. Pieper, A. Morell, F. Kools, *J. Mag. Mag. Mat*, 242-245 (2002) 1408-1410.

[20] R. Grössinger, C. Tellez Blanco, M. Küpferling, M. Müller, G. Wiesinger, *Physica B* 327 (2003) 202-207.

[21] S. E. Jacobo, C. Herme and P. G. Bercoff, "*Influence of the iron content on the formation process of substituted Co-Nd strontium hexaferrite prepared by the citrate precursor method"* JALCOM-S-08-02640, in press.

Figures' captions

Figure 1: X-ray diffraction patterns of the powders calcined at 800ºC for two hours.

Figure 2: X-ray diffraction patterns of the powders calcined at 1100ºC for two hours.

Figure 3: Room-temperature Mössbauer spectra of sample N30-1100. The different crystalline sites are indicated at the bottom.

Figure 4: Fe^{3+}occupancy of the five sites of $Sr_{1-x}Nd_xFe_{12(1-x)}Co_xO_{19}$. Theoretical values are given by open symbols connected by dashed lines for the different sites.

Figure 5: Isomer shift of the five sites of $Sr_{1-x}Nd_xFe_{12(1-x)}Co_xO_{19}$.

Figure 6: Quadrupole splitting of the five sites of $Sr_{1-x}Nd_xFe_{12(1-x)}Co_xO_{19}$.

Figure 7: Saturation magnetization M_S for all the samples treated at 800 and 1100ºC.

Figure 8: Coercivity *H*c for all the samples treated at 800 and 1100ºC. The arrows indicate samples N0 and N30 calcined at 1100ºC, whose hysteresis loops are shown in the inset.

Figure 9: Fitting of the susceptibilities corresponding to samples N0-1100 to N40-1100. In every case two peaks are needed to obtain a good agreement with the experimental data.

Figure 1

Click here to download high resolution image

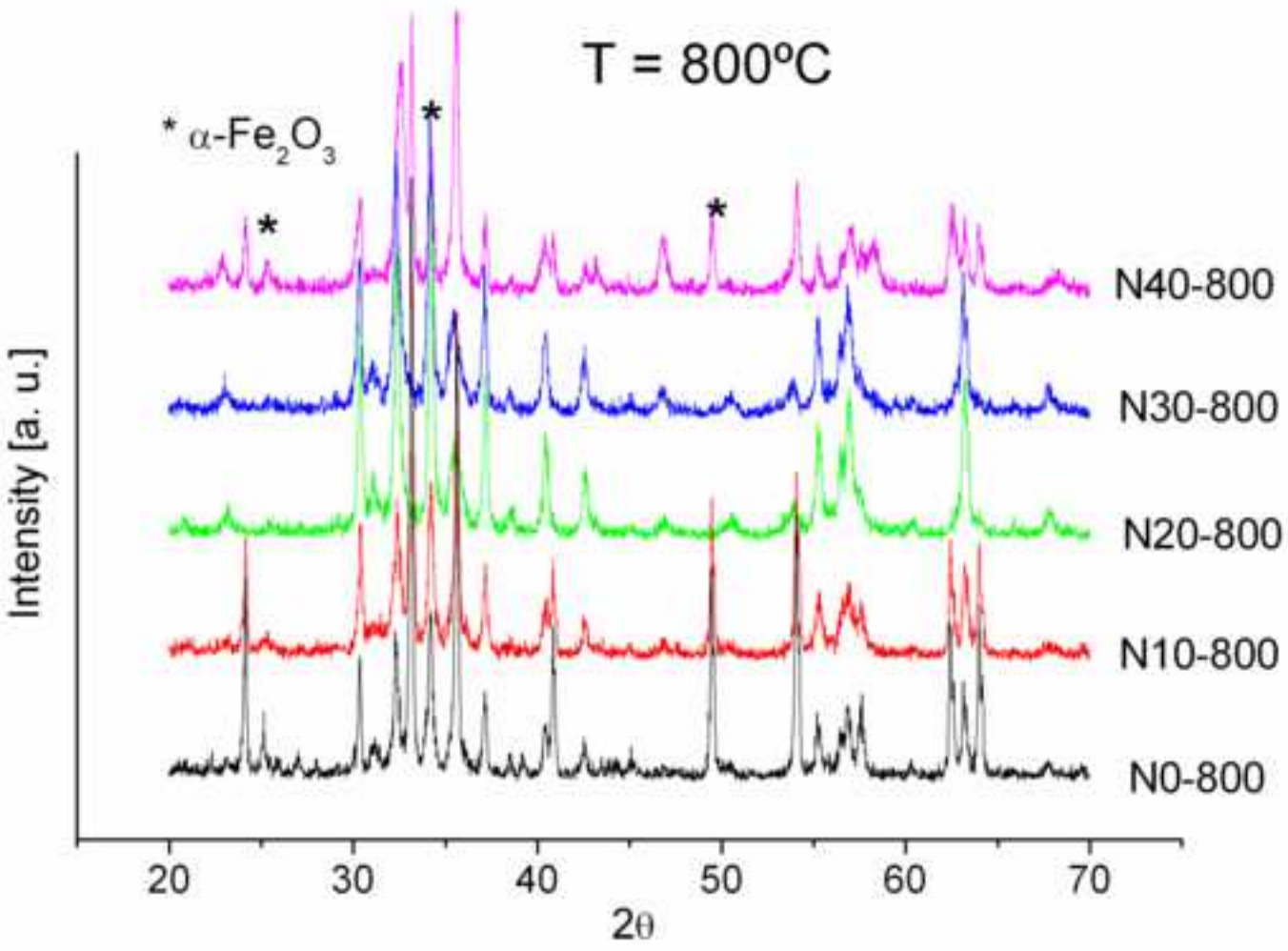

Figure 2

Click here to download high resolution image

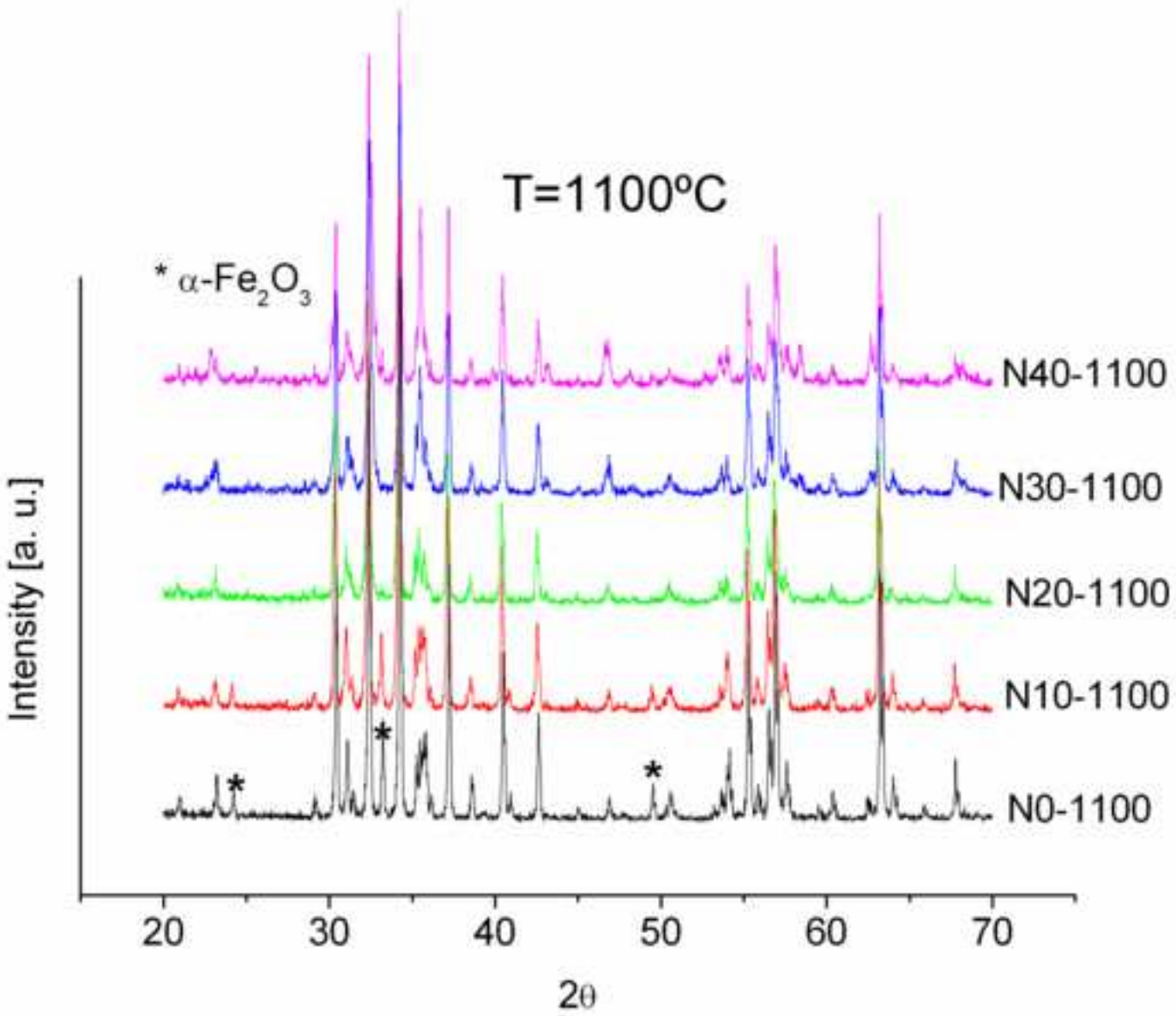

Figure 3

Click here to download high resolution image

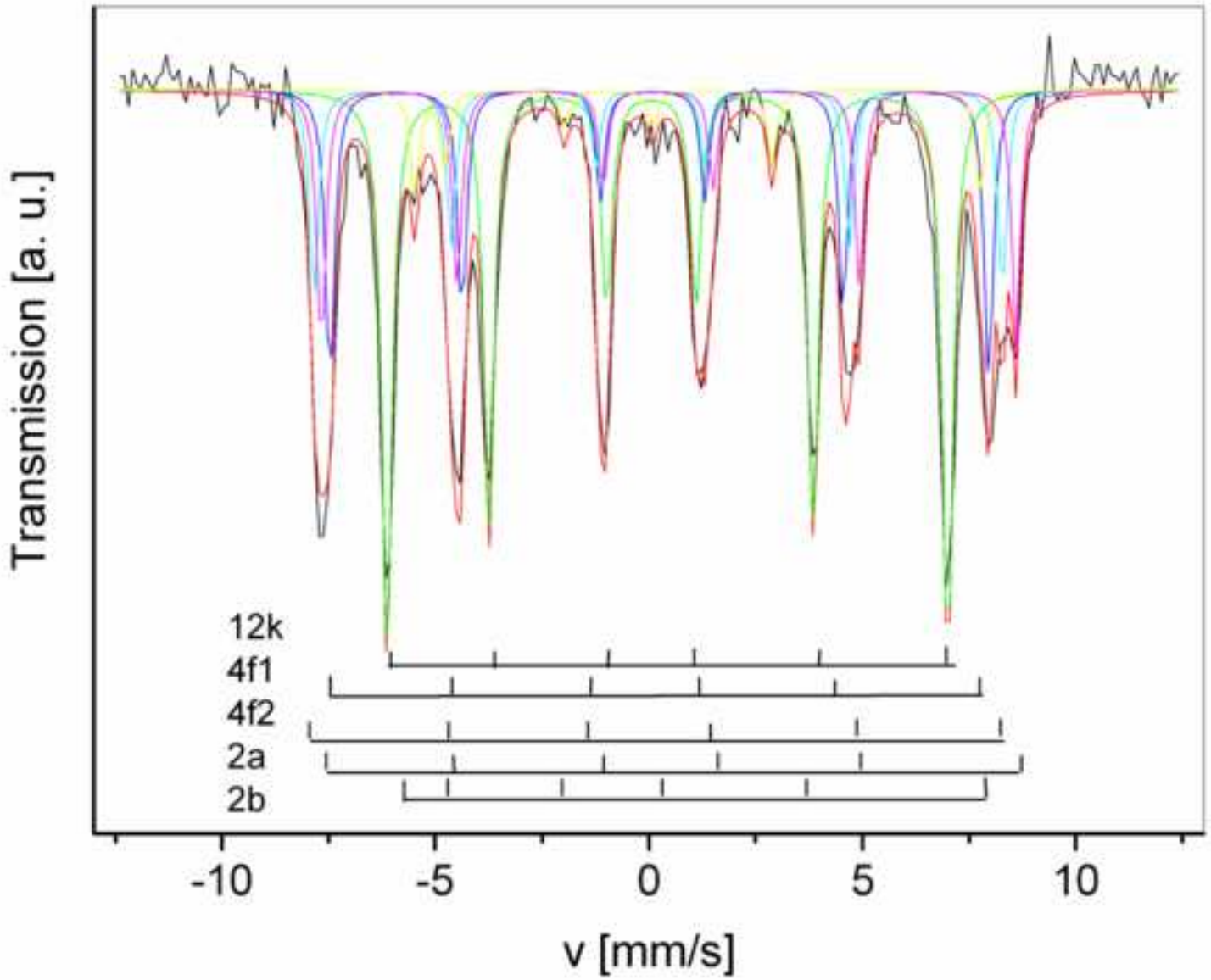

Figure 4

Click here to download high resolution image

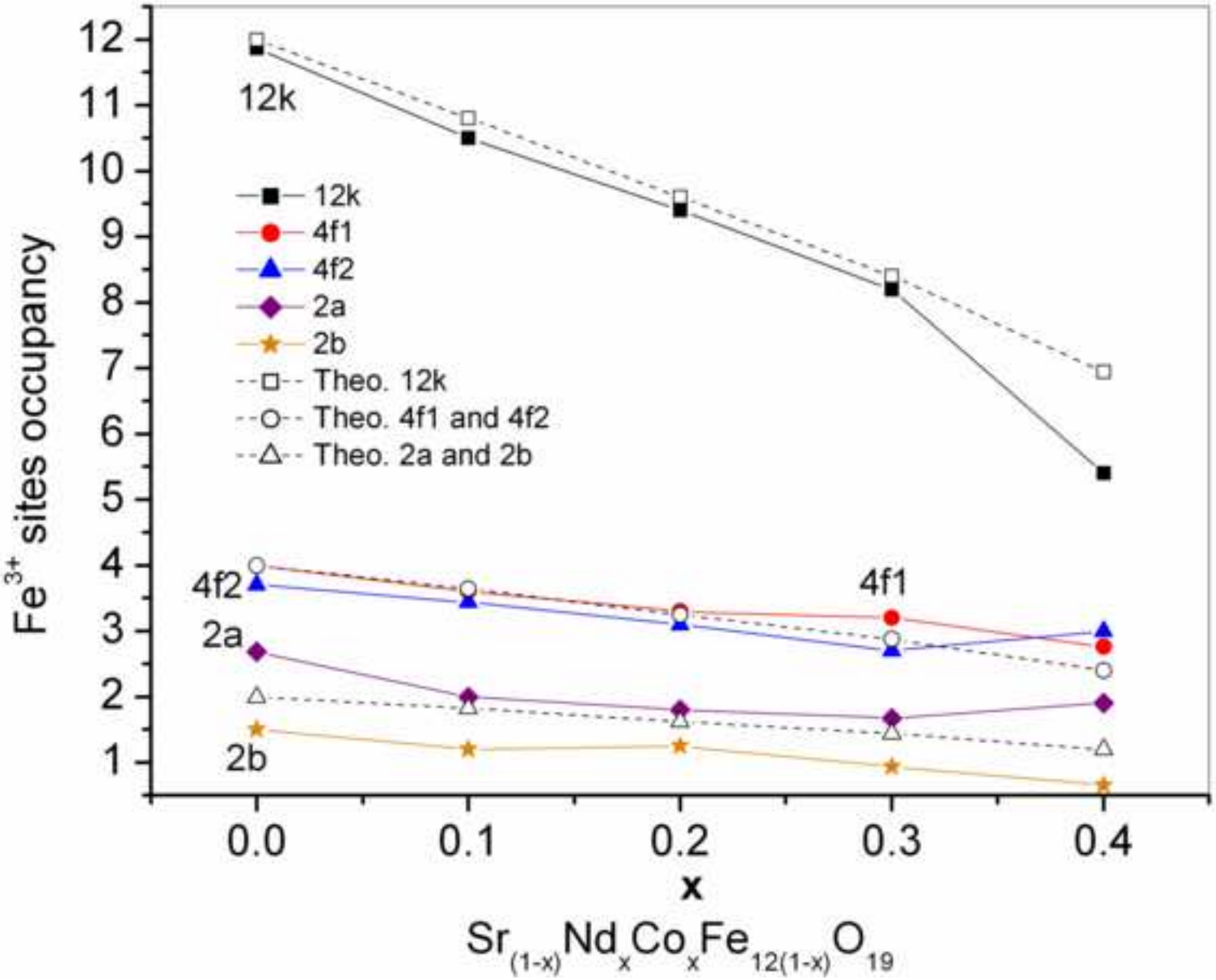

Figure 5

Click here to download high resolution image

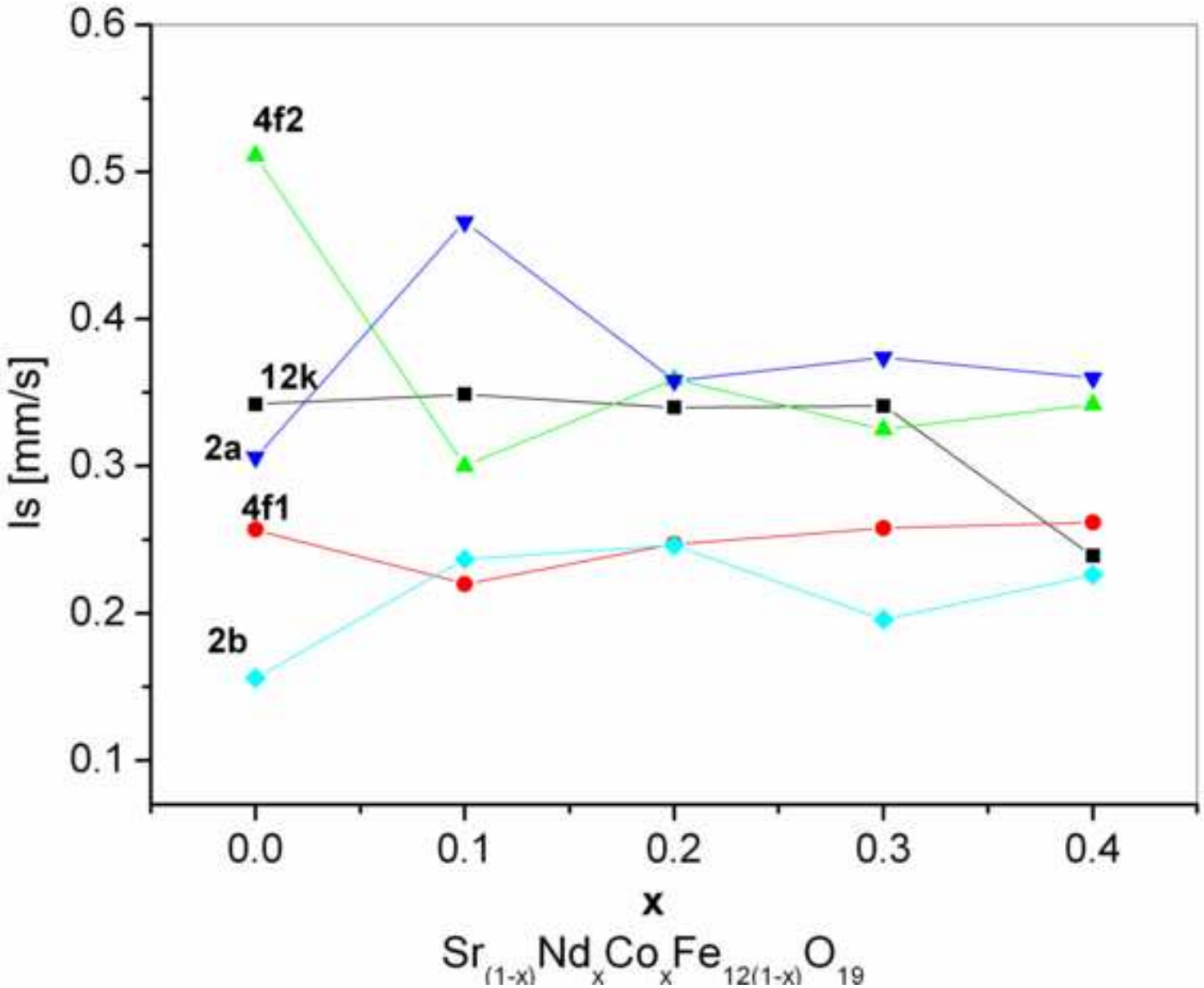

Figure 6

Click here to download high resolution image

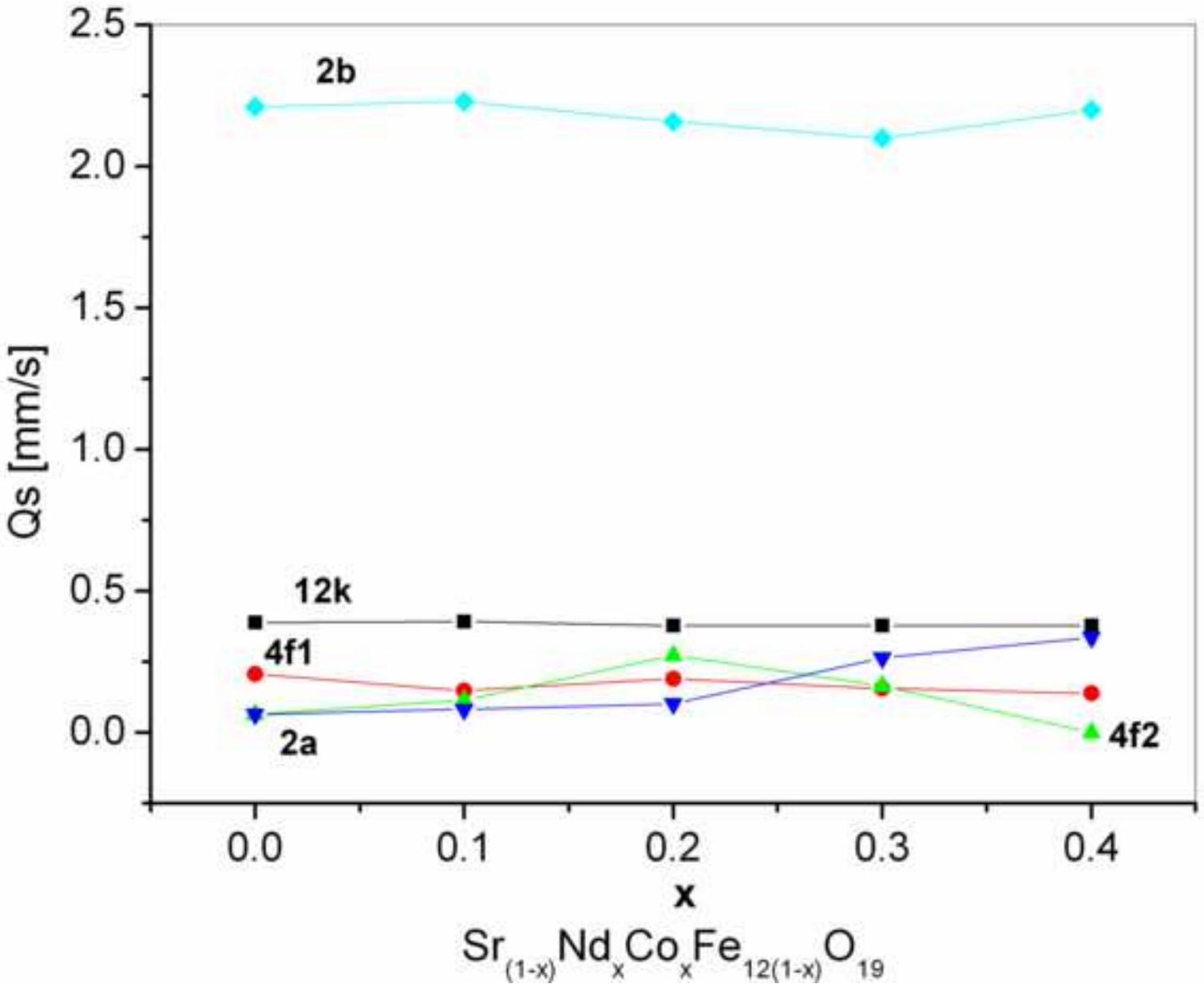

Figure 7

Click here to download high resolution image

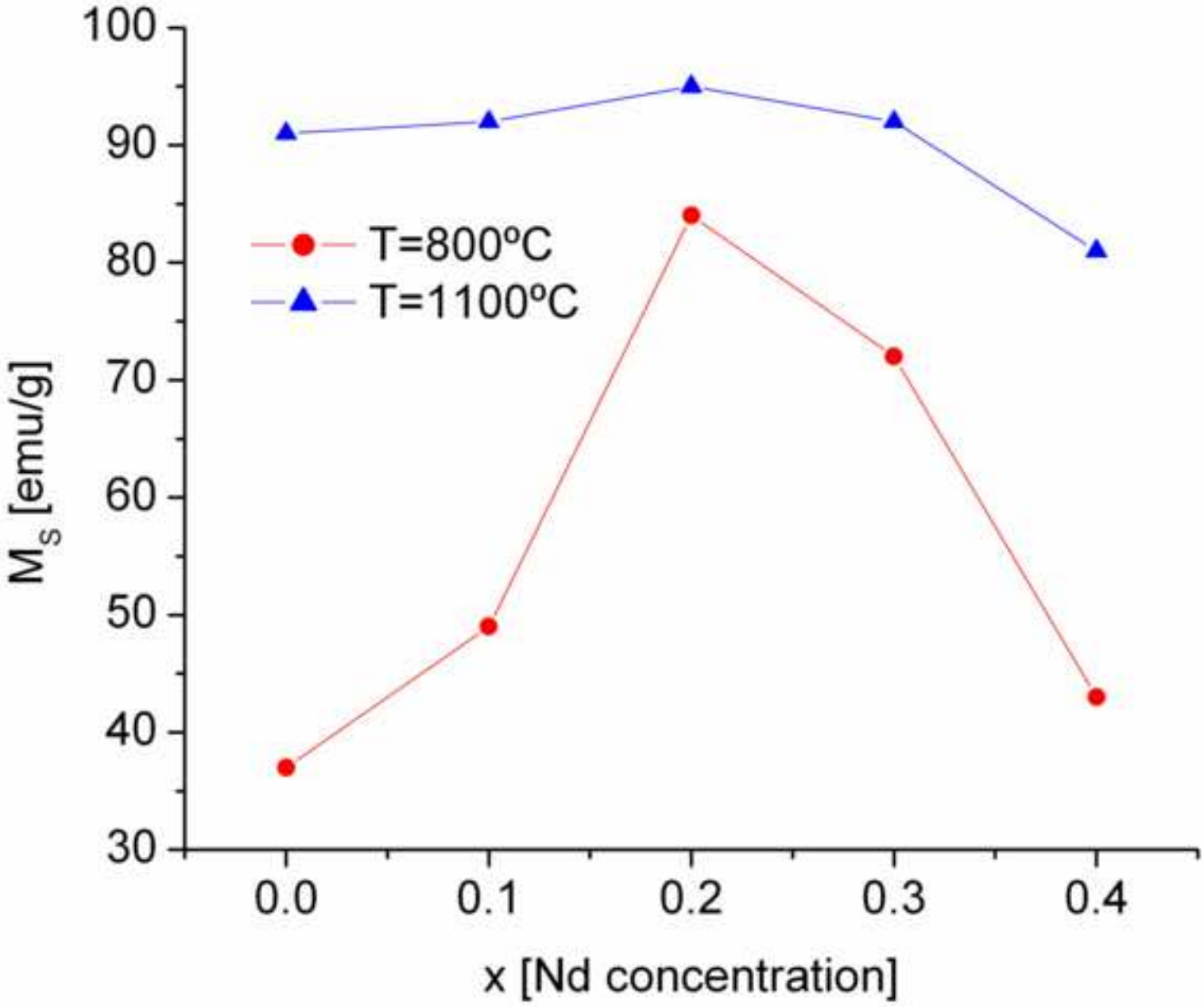

Figure 8

Click here to download high resolution image

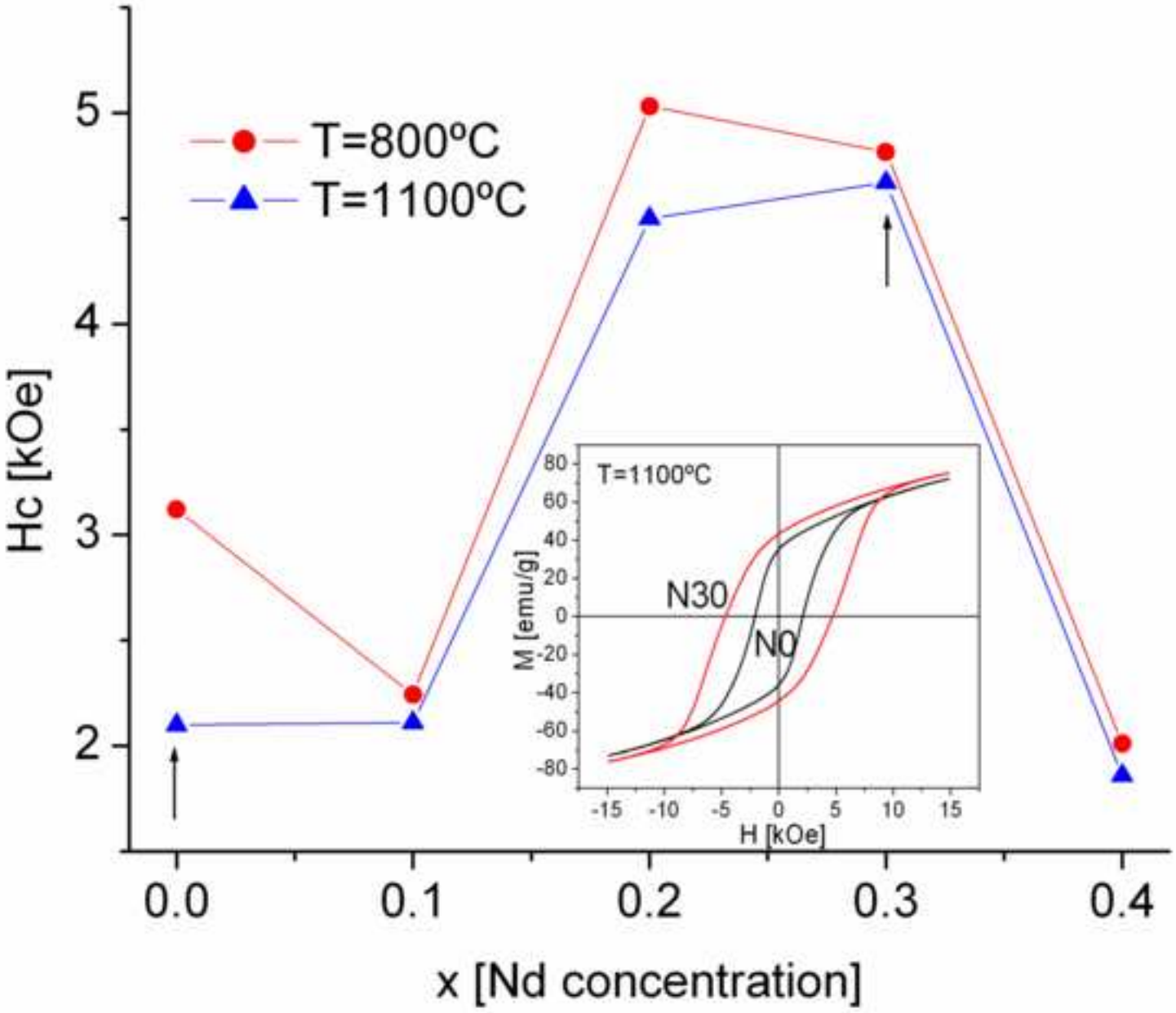

Figure 9

Click here to download high resolution image

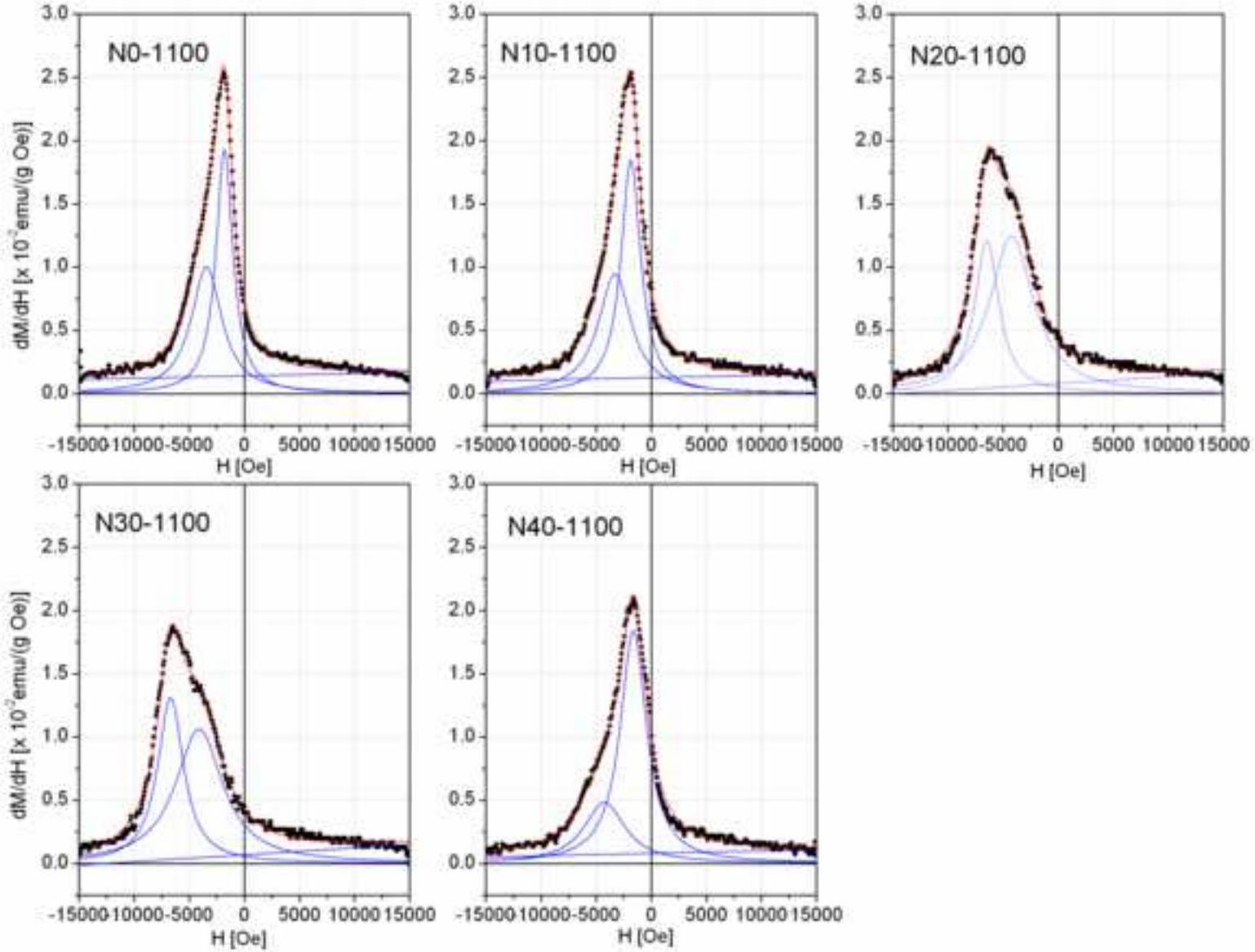

Table 1

Table 1: Composition, sample labels, calculated Fe vacancies, cell parameters and volume cell of powders calcined at 1100ºC.

Nominal composition	**Sample label**	Vacancies in Fe sites[a]	% Vacancy in Fe sites[b]	a [± 0.0008 Å]	c [±0.006 Å]	V [± 0.01 Å^3]
$Sr_1Fe_{12}CoO_{19}$	N0-1100	0	0	5.8747	22.990	687.14
$Sr_{0.9}Nd_{0.1}Fe_{10.8}Co_{0.1}O_{11.4}$	N10-1100	1.1	9.0	5.8795	23.052	690.12
$Sr_{0.8}Nd_{0.2}Fe_{9.6}Co_{0.2}O_{15.7}$	N20-1100	2.2	18.7	5.8841	23.049	691.10
$Sr_{0.7}Nd_{0.3}Fe_{8.4}Co_{0.3}O_{14.1}$	N30-1100	3.3	28.2	5.8845	23.043	691.01
$Sr_{0.6}Nd_{0.4}Fe_{6.9}Co_{0.4}O_{12.0}$	N40-1100	4.6	40.1	not hexagonal	not hexagonal	-

[a] Number of Fe atoms missing in the unit cell.

[b] % vacancy in Fe sites in a unit cell.

Table 2

Table 2: Magnetic values of all samples calcined at 1100ºC.

Sample	$M_{max\text{-}15kOe}$ **(± 0.5 emu/g)**	***M*s (± 0.5 emu/g)**	***H*c (± 5 Oe)**	**χ*H*c$_1$ (± 5 Oe)**	**χ*H*c$_2$ (± 5 Oe)**
N0-1100	72	91	2100	1810 (52%)	3430 (48%)
N10-1100	73	92	2110	1850 (55%)	3300 (45%)
N20-1100	76	95	4500	4220 (64%)	6480 (36%)
N30-1100	74	92	4670	4100 (59%)	6690 (41%)
N40-1100	66	81	1860	1620 (72%)	4240 (28%)